

# Quantum mechanical calculations of different monomeric structures with the same electroactive group to clarify the relationship between structure and ultimate optical and electrochemical properties of their conjugated polymers

Pinar Tunay Tasli<sup>a,\*\*</sup>, Tugba Soganci<sup>b</sup>, Sevgi Ozdemir Kart<sup>a</sup>, Hasan Huseyin Kart<sup>c</sup>, Metin Ak<sup>d,\*</sup>

<sup>a</sup> Pamukkale University, Physics Department, Campus, Denizli, Turkey

<sup>b</sup> Eskişehir Technical University, Graduate School of Sciences, Department of Advanced Technologies, Eskişehir, Turkey

<sup>c</sup> Aydın Adnan Menderes University, Physics Department, Aydın, Turkey

<sup>d</sup> Pamukkale University, Chemistry Department, Campus, Denizli, Turkey

## ARTICLE INFO

### Keywords:

Conducting polymers  
Spectroelectrochemistry  
Density functional theory calculations

## ABSTRACT

Quantum mechanical calculations can clarify the relationship between structure and ultimate optical and electrochemical properties of conjugated polymers and produce a ground for the design of advanced materials for futuristic applications. Herein, we have examined the structural geometries and electronic properties of different monomeric structures with the same electroactive group to provide a relationship between calculated electronic properties of the monomers with the observed optical and electrical properties of their conjugated polymers. For this purpose, three different amide substituted 2,5-di(2-thienyl)-1H-pyrrole compounds containing a different number of electroactive groups have been synthesized and molecular structure optimizations have been carried out with the Density Functional Theory (DFT) calculations. FT-IR and NMR spectra of optimized geometries have been compared with experimental data. Furthermore, electronic properties of the monomeric structures such as chemical hardness/softness, ionization potential, HOMO-LUMO energy levels, electronegativity have been revealed and molecular electrostatic potential (MEP) surface has been calculated to determine the electrophilic and nucleophilic reactive attack regions of the molecules considered in this study. Finally, Total Density of State (TDOS), Partial Density of State (PDOS) and Mulliken charge analyses of these molecules have been carried out. Our calculations based on ab-initio methods for the monomers have been compared with the optical and electrical properties of their conductive polymers in order to understand interrelationship between monomer structure and polymer properties.

## 1. Introduction

In recent years, conjugated polymers have been the focus of interest in fundamental and practical research due to their promising optical and electrical properties [1–7]. These  $\pi$ -conjugated systems which have alternating single ( $\sigma$ ) and double ( $\pi$ ) bonds exhibit inherently optical and electrical properties. Conjugated polymers with stable optical, mechanical and electrical properties are key components in many practical applications such as electrochromic devices [8–13], photovoltaic cells [14–16], light emitting diodes [17,18], biosensors [19–27], supercapacitors [28,29]. The most important factor for development in these

areas is understanding the tuning parameters of the electrochemical and optical properties of CPs. It is well known that the parameters that most affect the optical and electrochemical properties of conjugated polymers are their degree of crystallinity, conjugation length and intra-/inter-chain interactions [30,31]. These parameters can be controlled effectively with smart monomer design based on structure-property relationship approaches. In this point of view, quantum mechanical calculations have crucial role in designing of monomers and their conjugated polymers for desired optical and electrochemical properties [32–36].

Structure and spectroscopic properties of the chemical compounds

\* Corresponding author.

\*\* Corresponding author.

E-mail addresses: [ptunay@pau.edu.tr](mailto:ptunay@pau.edu.tr) (P.T. Tasli), [metinak@pau.edu.tr](mailto:metinak@pau.edu.tr) (M. Ak).

<https://doi.org/10.1016/j.jpcs.2020.109720>

Received 14 July 2020; Accepted 16 August 2020

Available online 28 September 2020

0022-3697/© 2020 Elsevier Ltd. All rights reserved.

are theoretically illuminated with quantum physics. The way quantum physics applying to chemical problems is called quantum chemistry. Computer-assisted quantum chemical calculations are used to predict the structural, spectroscopic and electronic properties of chemical materials without making any experimental studies [37]. The most important purpose of these programs is to determine the quantized energy levels of molecules, ions or nuclei by using spectroscopy. Then it is to calculate structural parameters, electrical-electronic properties and thermal properties using the forces and interactions between atoms, molecules or nuclei [38].

The future of conjugated polymers based on the ability of the theoretical and organic chemist to understand which synthetic modifications to existing and yet unknown conjugated polymers will result in the improvement of their optical and electrical properties [39–41]. Quantum chemistry calculations can clarify the relationship between structure and ultimate optical and electrochemical properties of conjugated polymers and produce a ground for the design of advanced materials for futuristic applications.

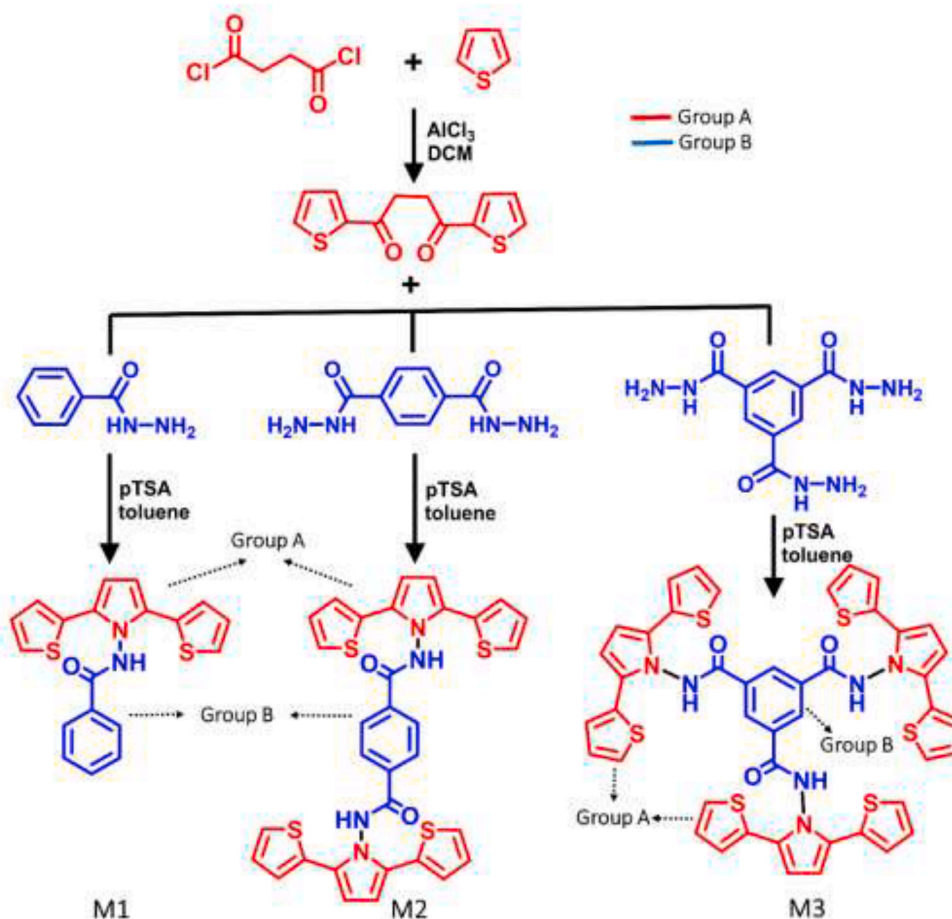
In this point of view, in this study we have examined the structural geometries and electronic properties of different monomeric structures with the same electroactive group to provide a relationship between the calculated electronic properties of the monomers and the observed optical and electrical properties of their conjugated polymers. For this purpose, three different amide substituted 2,5-di(2-thienyl)-1H-pyrrole compounds containing a different number of electroactive groups have been synthesized and molecular structure optimizations have been carried out with the Density Functional Theory (DFT) calculations. 2,5-Di(2-thienyl)-1H-pyrrole derivatives have been chosen because they have better optical and electrical properties than thiophene and pyrrole-based electroactive monomers [35,42–44]. Fourier Transform Infrared

(FT-IR) and Nuclear Magnetic Resonance (NMR) spectra of optimized geometries have been compared with experimental data. Furthermore, electronic properties of the monomeric structures such as chemical hardness/softness, ionization potential, highest occupied molecular orbital (HOMO)-lowest unoccupied molecular orbital (LUMO) energy levels, electronegativity have been revealed and molecular electrostatic potential (ESP) surface has been computed to determine the electrophilic and nucleophilic reactive attack regions of the investigated molecules. Finally, TDOS, PDOS and Mulliken charge analyses of the molecules have been carried out. Our ab-initio calculations of the monomers have been compared with the optical and electrical properties of their conductive polymers in order to understand interrelationship between monomer structure and polymer properties. Firstly, in this study, the structures of the molecules have been optimized by using DFT at the level of B3LYP with the basis set of 6–311G(d-) via Gaussian 09 W program [45]. Later, the structural and vibrational properties, NMR chemical shifts, molecular frontier orbital energies, electronic properties such as TDOS, PDOS analysis, Mulliken charge analysis, molecular ESP maps of the optimized molecular structure of title molecules are obtained theoretically. As a result, the experimental data of electrochromic materials have been supported by ab-initio calculations in this study. This work confirms that DFT computations allow us to better understand the nature of electrochromic materials.

## 2. Experimental

### 2.1. Synthesis and characterization of monomers

First of all, 1,4-di(2-thienyl)-1,4-butanedione has been synthesized by Friedel-Crafts Acylation reaction of thiophene and succinyl chloride



Scheme 1. Synthesis routes of M1, M2 and M3.

in presence of aluminum chloride. Details of this reaction can be found elsewhere [43,46,47]. The monomers have been obtained by the Knorr-Paal reaction of 1,4-di(2-thienyl)-1,4-butanedione and corresponding hydrazide derivative in toluene containing a catalytic amount of pTSA as specified in the literature (Scheme 1) [11,12,43]. Detailed synthesis procedures for monomers (*N*-(2,5-di(thiophen-2-yl)-1*H*-pyrrol-1-yl)benzamide as M1, *N*<sup>1</sup>,*N*<sup>4</sup>-bis(2,5-di(thiophen-2-yl)-1*H*-pyrrol-1-yl)terephthalamide as M2 and *N*<sup>1</sup>,*N*<sup>3</sup>,*N*<sup>5</sup>-tris(2,5-di(thiophen-2-yl)-1*H*-pyrrol-1-yl)benzene-1,3,5-tricarboxamide as M3) are given in Electronic Supporting Information (ESI). Furthermore, chemicals used in this research and instruments used for characterizations of the materials are mentioned in ESI.

## 2.2. Electrochemical and spectroelectrochemical processes

Electropolymerizations and electrochemical characterizations of monomer and corresponding polymers have been performed in three-electrode electrochemical cell at ambient temperature. Indium tin-oxide coated glass slides ( $R = 4\text{--}16 \Omega\text{sq}^{-1}$ ,  $0.7 \times 0.5 \times 0.07 \text{ cm}$ ), Ag/Ag<sup>+</sup> and platinum wire (% 99.99,  $0.01 \times 5 \text{ cm}$ ) have been used as working, reference and counter electrodes in electrochemical cell. The electrolyte solution used in the electropolymerization process is 0.1 M LiClO<sub>4</sub> and 0.01 M related monomer containing acetonitrile solution. Monomer-free electrolyte solution is used in all other electrochemical processes.

## 2.3. Structural characterization

The chemical structures of the monomers (M1-M3) have been confirmed by NMR spectral analyses. <sup>1</sup>H NMR and <sup>13</sup>C NMR spectra of monomers are recorded with Bruker-Instruments-NMR Spectrometer (DPX-400) operating at 400 MHz in the medium of dimethylsulfoxide (DMSO). PerkinElmer 2000 model an attenuated total reflectance Fourier transform infrared spectroscopy (ATR-FTIR) is used to identify the vibration modes of the synthesized monomers. The surface morphologies of corresponding polymer films on ITO electrode obtained by electropolymerization of the synthesized monomers was investigated by SEM images.

## 2.4. Theoretical methods

Imaging and calculation procedures of M1, M2 and M3 molecules are made with Gauss View 5.0.8 and Gaussian 0.9 programs, respectively [45,48]. Ab-initio simulations based on DFT/B3LYP/6-311G(d) method are performed to optimize the geometries of all molecules taking into account in this work. Then, the vibrational wave numbers of the main molecules by means of the optimized geometries are calculated using the same method. The vibration wave numbers calculated are scaled by 0.966 for 6-311G(d) basis set [49]. The marking of the vibration frequencies of the studied molecules is carried out by using the VEDA4 program (Vibrational Energy Distribution Analysis). Since experimental chemical shifts are performed in DMSO solution, the <sup>1</sup>H and <sup>13</sup>C NMR chemical shifts of the same molecules in the same solution are computed by using the Gauge-Independent Atomic Orbital (GIAO) approach applying DFT/B3LYP method with the basis set of 6-311G(d) [50]. In the next step, the electronic properties such as chemical hardness, chemical softness, ionization potential, electron affinity, electronegativity, electrophilicity and chemical potential of the conductive polymers considered are investigated by utilizing the HOMO-LUMO energies. Theoretically, the molecular ESP surface is used to determine the electrophilic and nucleophilic reactive attack regions of the molecules. Then, Mulliken charge analyses of conductive polymers are performed. Finally, the TDOS and PDOS analyses are evaluated to clarify the electronic properties.

## 3. Results and discussion

### 3.1. Geometrical structure

The three-dimensional approximate geometry of the studied molecules in the ground state has been visualized by the GaussView 5.0.8 molecular viewing program and the simulations of the structural, spectroscopic and electronic properties of molecules are achieved via Gaussian 09 package program in the gas phase [45,48]. These calculations have been succeeded using the Density Function Theory/Becke-3-Lee-Yang-Parr (DFT/B3LYP) method with the 6-311G(d) basis set [50,51]. The atom numbering schemes and the optimized structures of the M1, M2 and M3 molecules obtained from DFT/B3LYP/6-311G(d) methods are given in Fig. 1. The dihedral angles of the selected regions (yellow part in Fig. 1) in the optimized molecules are given in Table 1. The band gap of a conducting polymer can be expressed by the sum of the five contributions denoted as bond length alternation, planarity, resonance energy, substitution, intermolecular effects [52]. Considering that all effects except planarity in the three molecules tackled are approximately similar each other, the most important feature in these molecules is the planarity of the 2,5-di(2-thienyl)-1*H*-pyrrole groups. With the aim of determining the planarity of all molecules, dihedral angles of the atoms in the 2,5-di(2-thienyl)-1*H*-pyrrole groups of all three molecules are calculated. The dihedral angles of optimized structures show that the molecule M3 is more planar as compared to the molecules of M1 and M2. In order to characterize the molecular structures of the M1, M2 and M3 molecules, 41, 70 and 99 bond lengths, 65, 112 and 159 bond angles and 96, 167 and 241 dihedral angles are necessary, respectively. All these bond lengths, bond angles and dihedral angles are given in Tables S1, S2 and S3, respectively, as a supplementary data in ESI.

### 3.2. Vibrational spectrum analysis

Vibrational spectroscopy is a non-destructive identification method that measures the vibrational energy of a compound. The binding sites and the state of bonds in the structure, the functional groups of organic compounds in the form of solid, liquid and solution can be determined with the use of FT-IR Spectrometer. The experimental vibrational spectra of three molecules have been measured by FT-IR Spectrometer. The vibrational spectra of our molecules are calculated by using DFT/B3LYP method with 6-311G(d) basis set. It is known that a non-linear molecule with *N* atoms has 3*N*-6 normal modes of vibration. The molecules of M1, M2 and M3 have 38, 64 and 90 atoms, and 108, 186 and 264 fundamental vibrational modes, respectively. Of the 108 vibrational normal modes for M1 molecule, 37 modes are stretching vibration, 36 modes are bending and the remaining 35 modes are torsional vibrations. There are 63 stretching, 62 bending and 61 torsional modes for M2 molecule, while M3 has 89 stretching, 88 bending and 87 torsional of the fundamental modes. M1, M2 and M3 molecules have 39, 60, and 81 C-H vibrational modes, respectively. The vibration frequencies of the molecules computed from DFT/B3LYP method with 6-311G(d) basis set are in better agreement with the experiment when multiplied by the scale factor of 0.966 [53]. Later, these normal modes of vibration are marked with Gaussian 5.0.8 and VEDA4 program [49]. The FT-IR spectra computed from DFT/B3LYP method with 6-311G(d) basis set and those measured for M1, M2 and M3 are plotted in Fig. 2 (a), (b) and (c), respectively. The all vibrational wavenumbers and IR intensity calculated from DFT and the assignments of IR vibration modes to characterize the M1, M2 and M3 molecules are given in Tables S4, S5 and S6 as supplementary materials provided in ESI. For the M1, M2 and M3 molecules, the N-H stretching vibrations are recorded at range of 3477–3497 cm<sup>-1</sup> in theoretical calculations. According to PED analysis, these modes are almost pure N-H stretching vibrations (PED, 100%) for all molecules. The C=O band and aromatic C-H band are in the range of 1706–1726 cm<sup>-1</sup> and 3070–3106 cm<sup>-1</sup>, respectively. The

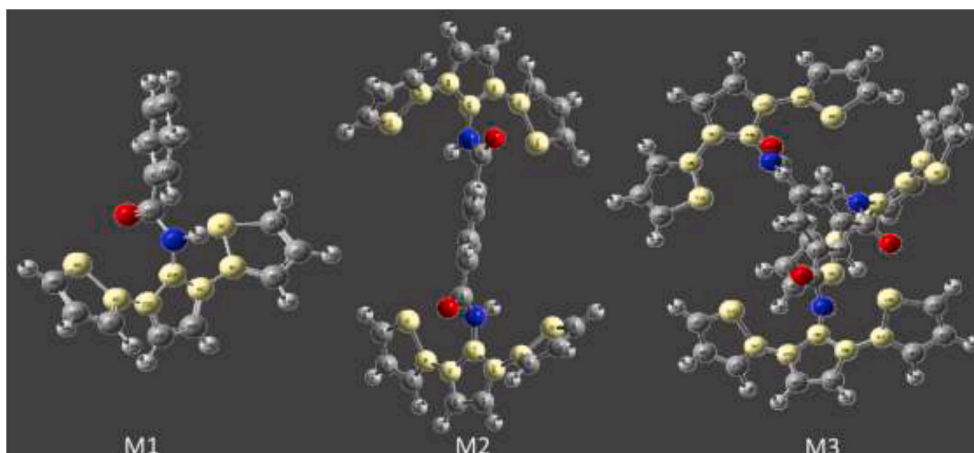


Fig. 1. The optimized molecular structures obtained from DFT/B3LYP/6-311G(d) method for the molecules M1, M2 and M3.

**Table 1**

Dihedral angles of the optimized structures of chemical compounds M1, M2 and M3 at the B3LYP/6-311G(d) level of theory.

Dihedral Angles ( $^{\circ}$ )	DFT/B3LYP/6-311G(d)		
	M1	M2	M3
N21–C22–C8–S9	47.991	–46.276	48.102
N21–C6–C4–S3	–52.033	–31.245	–52.587
N39–C30–C28–S27	–	–31.236	–50.704
N39–C40–C32–S33	–	–46.263	49.416
N57–C58–C50–S51	–	–	38.850
N57–C48–C46–S45	–	–	–47.225

experimentally FT-IR spectra of monomers are investigated between 4000 and 400  $\text{cm}^{-1}$ . Since the functional groups in all three molecules examined are identical, the FT-IR spectrum is also very similar as expected. The bands of the N–H stretching vibrations of all three molecules are observed at the wavenumbers of 3876  $\text{cm}^{-1}$ , 3737  $\text{cm}^{-1}$  and 3567  $\text{cm}^{-1}$  while C=O stretching vibrations are observed as very strong band at 1679  $\text{cm}^{-1}$  in FT-IR spectra. The peak at 1611  $\text{cm}^{-1}$  is attributed to C=C stretching vibration as C–C stretching, out-of plane bending, in-plane-bending and torsion vibrations modes observed at 1611–1453  $\text{cm}^{-1}$ . The theoretical vibration frequencies obtained from the DFT calculations of the molecules show good agreement with the experimentally observed vibrations. The correlation graphs between the experimental and the calculated frequencies are shown in Fig. 3 for M1,

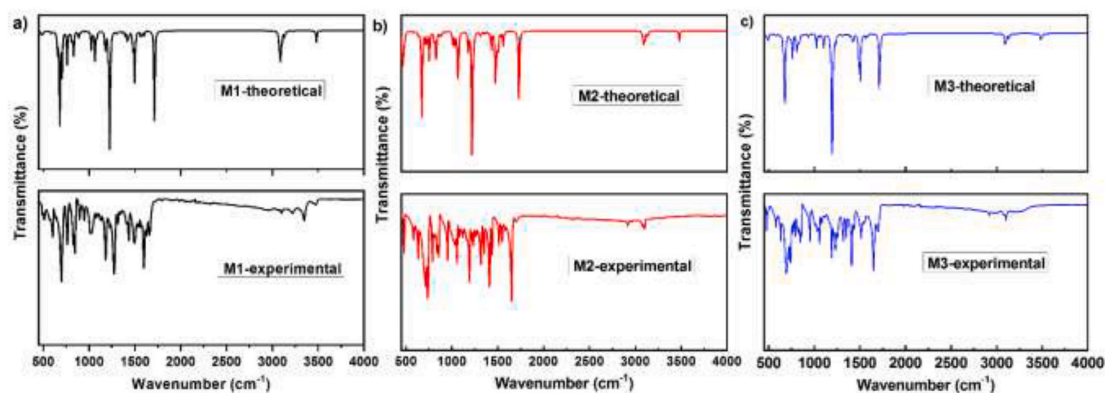


Fig. 2. The calculated and experimental infrared spectra (FT-IR) of M1, M2, and M3 molecules, respectively.

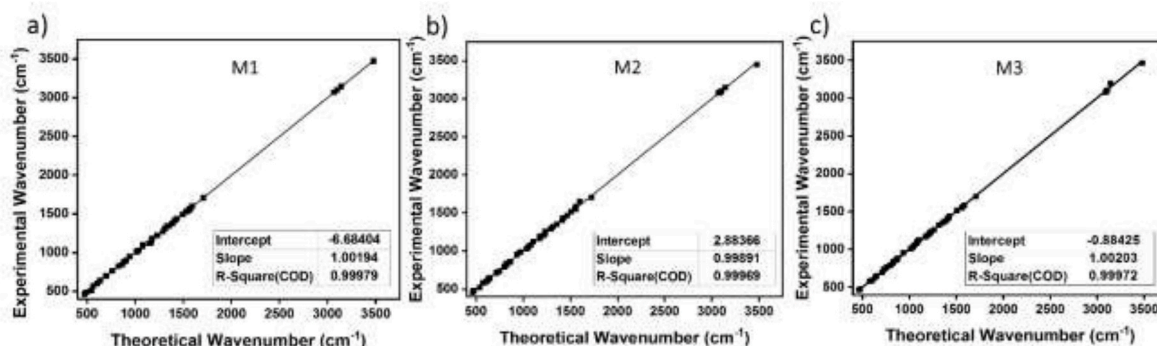


Fig. 3. The regression analysis of experimental and theoretical wavenumber predicted from DFT method for a) M1 b) M2 c) M3 molecules, respectively.

M2 and M3 molecules. Respectively, the correlation values ( $R^2$ ) between the theoretical and experimental vibration bands are found to be 0.99979, 0.99968, and 0.99971 for M1, M2 and M3 molecules.

### 3.3. $^1\text{H}$ and $^{13}\text{C}$ NMR spectra

Nuclear Magnetic Resonance (NMR) spectroscopy is an analytical chemistry technique used to determine the molecular structure, purity and content of a material in the solvent [54,55]. The NMR ( $^1\text{H}$  and  $^{13}\text{C}$ ) chemical shift values of the synthesized molecules are calculated using the GIAO approach at the level of DFT/B3LYP with 6-311G(d) basis set in DMSO solvent. The  $^1\text{H}$  and  $^{13}\text{C}$  NMR spectra of M1, M2 and M3 molecules are recorded in the medium of DMSO. The observed  $^1\text{H}$  and  $^{13}\text{C}$  NMR spectra of M1, M2 and M3 molecules (with respect to TMS, and in DMSO solution) are given in Fig. S1 as a supplementary material in ESI. The results of both experimental and theoretical  $^1\text{H}$  and  $^{13}\text{C}$  NMR for the molecules of M1, M2 and M3 are given in Table 2.

The linear correlation coefficients ( $R^2$ ) are obtained by using the values of experimental and computational  $^1\text{H}$  and  $^{13}\text{C}$  NMR chemical shift. The linear correlations graphs of  $^1\text{H}$  and  $^{13}\text{C}$  NMR chemical shift for M1, M2 and M3 molecules are given in Fig. S2 as a supplementary material in ESI. The correlation values ( $R^2 = 0.76384, 0.97564$  and  $0.9093$ ) between the experimental and calculated  $^1\text{H}$  chemical shifts for the DFT/B3LYP level are good in the solvent of DMSO for M1, M2 and M3 molecules. As interested in  $^{13}\text{C}$  chemical shifts, the correlations between the experimental and calculation are obtained as  $R^2 = 0.97292, 0.93409$  and  $0.90207$  for M1, M2 and M3 electroactive monomers, respectively. When the experimental and theoretical NMR results are compared, it is seen that the DFT/B3LYP method is versatile tool in examining the NMR properties of the electroactive materials.

### 3.4. Analysis of FMOs

The Molecular Orbital (MO) theory is a method used in chemistry to determine the electronic structures of molecules by utilizing quantum mechanics. The Frontier Molecular Orbital Theory (FMO) is an application of MO theory that determines the HOMO-LUMO interaction. According to the FMO theory, it is concluded that good approaches to reactivity can be found by analyzing the HOMO-LUMO interactions of the molecules. As a result, chemical reactions of molecules can be managed by examining FMO behaviors. Obtaining the difference between the HOMO-LUMO energies of the molecules causes the reaction between the molecules to be easy [56]. By looking at information about

chemical hardness and softness parameters, charge distribution, bond degree, electrostatic potential and molecular orbital shapes can be attained by exploring the electron density distributions of molecules. The ionization potential energy ( $I = -E_{\text{HOMO}}$ ) is the minimum energy required to remove an electron from the molecule in the gas phase. When an electron is added to the molecule in the gas phase, the increasing amount of energy gives the electron affinity ( $A = -E_{\text{LUMO}}$ ). Electronegativity ( $\chi = \frac{I+A}{2}$ ) is the power of an atom in a molecule to attract electrons. Chemical hardness ( $\eta = \frac{I-A}{2}$ ) is a measure of the inhibition of charge transfer in the molecule. Global electrophilicity index ( $\omega = \mu^2/2\eta$ ) can be explained by using Koopmans theorem [57]. If the value of chemical hardness is high, the charge transfer within the molecule is very low [58]. If the HOMO-LUMO energy difference of molecule is small, the electron distribution can be easily guided and large polarization is obtained. The electronic structure parameters of the molecules such as the ionization potential, electron affinity, global electronegativity, global electrophilicity, chemical hardness, chemical potential and global softness are calculated by means of DFT/B3LYP with 6-311G(d) basis set. The calculated electronic structure parameters of the compounds are given in Table 3. The molecule M3 is the best acceptor since it has the biggest electronegativity. Moreover, M3 is the most electrophile since the electrophilic value of M3 molecule is greater than other molecules. The energy difference of HOMO-LUMO ( $\Delta E$ ) is 3.954; 3.213 and 3.307 eV, respectively, for molecules M1, M2 and M3, which reflects that the values greater than 1.5 eV get the molecules thermodynamically stable and durable. In addition, the molecule doesn't react with itself, does not dimerize and polymerize. The HOMO-LUMO energy difference of the M1 molecule is higher than the other molecules. Therefore, M1 molecule becomes harder and less chemical reactive than other molecules. Low electron flow occurs due to its high energy difference. This cause M1 molecule to be low reactive. The electron density increases from green to red according to the electrostatic potential drawing. The atoms located at the HOMO-LUMO orbitals are very important since chemical reactions occur in the HOMO-LUMO orbitals. The HOMO-LUMO representations of M1, M2 and M3 molecules are calculated by DFT/B3LYP/6-311G(d) method and shown in Fig. 4.

### 3.5. ESP analysis

Electrostatic potential maps, also known as molecular electrical potential surface, show the charge distributions of molecules in three-dimensional structure. This map monitoring the charge distributions

**Table 2**

The theoretical and available experimental  $^1\text{H}$  NMR (d, ppm, DMSO- $d_6$ ) and  $^{13}\text{C}$  NMR (d, ppm, DMSO- $d_6$ ) values for M1, M2, and M3 molecules, respectively.

M1			M2			M3		
Atom Label	DFT	Exp.	Atom Label	DFT	Exp.	Atom Label	DFT	Exp.
H37 (a)	6.60	6.10	H54 (a)	6.62	6.22	H71 (a)	6.58	6.82
H28 (b)	7.25	6.72	H48 (b)	7.06	6.67	H61 (b)	7.29	7.25
H30 (c)		6.64						
H33 (d)	7.59	7.43	H46 (c)	7.32	6.83	H63 (c)	7.39	7.40
H29 (e)	7.76	6.86	H47 (d)	7.42	6.80	H65 (d)	7.97	7.53
H32 (f)	7.90	7.30	H49 (e)	8.17	7.58	H67 (e)	8.83	8.69
H31 (g)	8.03	7.49	H53 (f)	12.25	7.21	H70 (f)	12.48	7.79
H36 (h)	9.38	6.62	C24 (a)	107.64	111.91	C23 (a)	123.63	113.50
C23 (a)	107.95	113.34	C14 (b)	124.41	130.48	C5 (b)	129.31	130.49
C18 (b)	124.36	131.29	C5 (c)	127.22	128.24	C1 (c)	130.27	129.13
C7 (c)	127.22	130.92	C1 (d)	127.66	129.02	C14 (d)	133.88	134.45
C11 (d)	127.66	129.00	C10 (e)	127.82	133.51	C2 (e)	134.59	134.71
C10 (e)	128.09	134.91	C6 (f)	128.64	135.93	C6 (f)	140.40	137.78
C17 (f)	128.81	132.08	C4 (g)	128.92	141.73	C13 (g)	143.83	136.50
C6 (g)	132.15	137.30	C12 (h)	132.64	170.29	C4 (h)	153.44	142.00
C16 (h)	133.66	136.92	C13 (i)	135.48	140.43	C12 (i)	191.91	169.87
C8 (i)	143.61	142.18	C17 (k)	165.23	133.48			
C12 (j)	191.46	174.34						

Labels of the atoms in this Table are given according to Fig. 1 used in the assignment of the chemical shifts for M1, M2 and M3 molecules.

**Table 3**

Calculated electronic structure parameters and measured optical and electrochemical properties of the M1, M2 and M3 molecules.

DFT/B3LYP/6-311G(d)	M1	M2	M3
$E_{\text{HOMO}}$ (eV)*	-5.373	-5.329	-5.421
$E_{\text{LUMO}}$ (eV)*	-1.419	-2.116	-2.114
$E_g$ (eV)*	3.954	3.213	3.307
$I$ (eV)*	5.373	5.329	5.421
$A$ (eV)*	1.419	2.116	2.114
$\chi$ (eV)*	3.396	3.722	3.768
$\eta$ (eV)*	1.977	1.606	1.654
$\mu$ (eV)*	-3.396	-3.722	-3.768
$S$ (eV <sup>-1</sup> )*	0.253	0.311	0.302
$\omega$ (eV <sup>-1</sup> )*	11.398	11.129	11.735
Planarity of Group A*	High	Moderate	Highest
Donor character of Group A*	High	Moderate	Highest
$E_{\text{monset}}$ (V)**	0.62	0.72	0.60
$E_{\text{monox}}$ (V)**	0.93	1.18	0.87
$E_{\text{ponset}}$ (V)**	0.22	0.31	0.18
$E_{\text{pox}}$ (V)**	0.54	0.65	0.46
$Q_p$ (mC/cm <sup>2</sup> )**	1.877	1.741	3.265
$\Delta T_{\pi-\pi^*}$ (%)**	15 (430 nm)	41 (431 nm)	21 (414 nm)
$\Delta T_{\text{bipolaron}}$ (%)**	32 (906 nm)	94 (870 nm)	65 (920 nm)
$E_{g_p}$ (eV)**	2.10	2.28	2.21

\*obtained from DFT calculations \*\*obtained from electrochemical and optical measurements, ( $E_g$ ): band gap energy ( $I$ ): ionization potential, ( $A$ ): electron affinity, ( $\chi$ ): global electronegativity, ( $\eta$ ): chemical hardness, ( $\mu$ ): chemical potential and ( $S$ ): global softness, ( $\omega$ ): global electrophilicity, ( $E_{\text{monset}}$ ): Onset potential ( $E_{\text{monox}}$ ): Monomer oxidation peak potential, ( $E_{\text{ponset}}$ ): Polymer onset oxidation potential, ( $E_{\text{pox}}$ ): Polymer oxidation peak potential, ( $Q_p$ ): Polymer charge density, ( $\Delta T_{\pi-\pi^*}$ ): Optical contrast at  $\lambda_{\text{max}}$  for  $\pi-\pi^*$  transitions, ( $\Delta T_{\text{bipolaron}}$ ): Optical contrast at bipolaron transitions  $E_{g_p}$ : Polymer optical band gap calculated from  $1240/\lambda_{\text{max}}$

of molecules conducts how molecules interact with other molecules. The molecular electrostatic potential provides important information about the determination of regions where electrophilic and the nucleophilic reactions may take place in the molecule and the formation of intramolecular hydrogen bonds [59,60]. In an ESP map, the electron density of the molecule appears to change from red to blue. The electron-rich (red) region where the molecule repels the outer electrons has low potential energy. On the other hand, the electron-poor (blue) region where the molecule attracts the outer electrons (this region is positively charged) has high potential energy. The green regions on the ESP map has the neutral electrostatic potential is neutral points. In addition, the orange-yellow and light blue regions on the map show partial negative or positive charges. ESP maps of M1, M2 and M3 molecules in the optimized geometries are achieved by utilizing DFT/B3LYP/6-311G(d) method. The electrophilic and nucleophilic regions obtained from the ESP maps are illustrated in Fig. 5 Electrostatic potential values on the surface of M1, M2 and M3 molecules vary in the range of  $\pm 0.06073$  a.u.,  $\pm 0.05778$  a.u. and  $\pm 0.05515$  a.u., respectively. As seen in Fig. 5, while the electron-rich regions are formed around O atoms, the electron-poor regions are created around N-H groups for the M1, M2 and M3 molecules. Additionally, the regions where H atoms are located in are also positive area on the ESP maps. These regions consisting of electron density indicate the position where molecules have the ability of metallic bonds [61].

### 3.6. Investigation of Mulliken charge

Mulliken charge distribution is one of the most used charge analysis methods. Mulliken charge analysis are used to estimate qualitatively the experimental results [62–64]. Mulliken atomic charges are predicted by

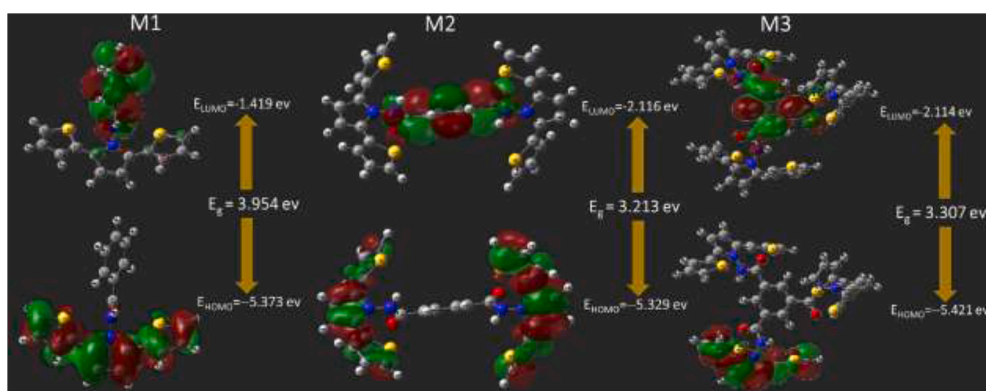


Fig. 4. The schema displaying the frontier molecular orbitals (HOMO and LUMO) computed via DFT/B3LYP method in the gas phase for M1, M2 and M3 molecules.

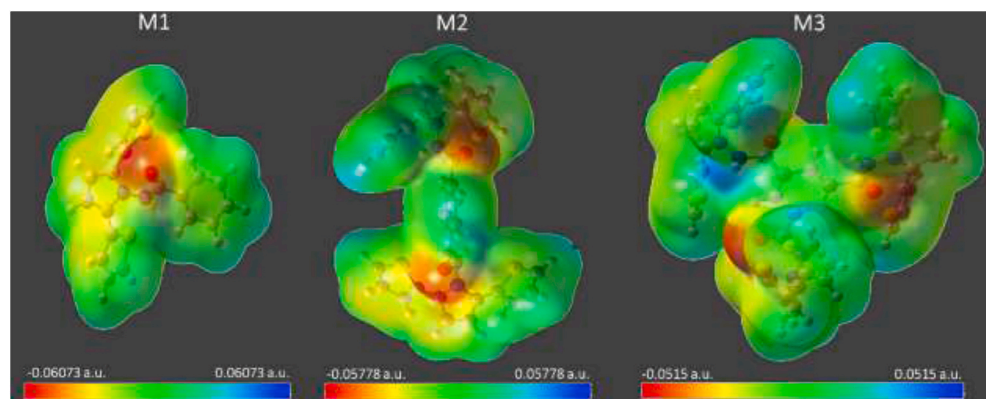


Fig. 5. The isosurface total electron density mapped with the use of molecular electrostatic potential of M1, M2 and M3 molecules by using the method of DFT at the level of B3LYP.

using the DFT/B3LYP/6-311G(d) method to investigate the electron population of each atom in organic molecules. Mulliken atomic charges of each atom are obtained for M1, M2 and M3 molecules. Mulliken atomic charges for the selected atoms groups in each molecule are given in Fig. 6.

It is reported from the Mulliken analysis that C atoms bound to O and N atoms are positively charged, while C atoms bound to the H atoms are negatively charged. It is seen that mostly C atoms have a negative atomic charge as expressed in Ref. [65]. All H and S atoms in the molecules have a positive charge while O and N atoms have a negative charge.

### 3.7. TDOS and PDOS analysis

The function of density of states describes the number of available states in a system and is essential for determining the carrier concentrations and energy distributions of carriers with in compounds. The partial density of state shows the contribution of the specific atomic groups or functional groups selected in the compounds to each of molecular orbital. In this part of our study, the density of states spectra of three molecules are obtained. The TDOS, PDOS and band structures of the title molecules are calculated using the GaussSum 3.0 program with Gaussian curves of unit height and full width at half maximum (FWHM) of 0.3 eV. The representation of TDOS, PDOS and band are given in Fig. 7. In the TDOS graphs, the pink colored region shows the HOMO orbital, while the green colored region shows the LUMO orbital. The PDOS is used to find bonding, anti-bonding and non-bonding properties according to certain fragments. While the positive region indicates the binding interaction in molecules, the anti-bonding interaction indicates that negative values and non-bonding interactions are closed to zero [66,67]. It is seen in the PDOS plots that the orbitals of the determined atoms in the molecules contribute to the molecular orbitals. The TDOS of HOMO for the M1, M2 and M3 molecules mostly comes from PDOS of selected group A in the molecules. These values are 99%, 100% and 100% for M1, M2 and M3 molecules, respectively. On the other hand, the LUMO is mainly composed of PDOS of selected group B in title

molecules. These values are 97%, 99% and 98% for M1, M2 and M3 molecules, respectively. In addition, the contribution of group A to the PDOS of LUMO+1 for the M1 molecule is 88% while the contribution of group B is 12%. For M2, the contribution of group A to the PDOS of LUMO+1 is 85% while the contribution of group B is 15%. While the contribution of group A to the PDOS of LUMO+2 for the M3 molecule is 93% while the contribution of group B is 7%. Generally, the TDOS of LUMO + mostly comes from PDOS of group A of M3 molecule.

### 3.8. Electrochemical and spectroelectrochemical properties

Electropolymerizations and electrochemical characterizations of monomer and corresponding polymers have been performed in three-electrode electrochemical cell at ambient temperature. Indium tin-oxide coated glass slides, Ag/Ag<sup>+</sup> and platinum wire have been used as working, reference and counter electrodes in electrochemical cell. The electrolyte solution used in the electropolymerization process is 0.1 M LiClO<sub>4</sub> and 0.01 M related monomer containing acetonitrile solution. Monomer-free electrolyte solution is used in spectroelectrochemical processes. In spectrophotometric analysis, the changes in the optical properties of the polymer under applied potentials with a potentiostat were examined simultaneously with an UV spectrophotometer. Electrochemical properties and electropolymerizations of electroactive molecules called M1, M2 and M3 have been investigated by cyclic voltammetry technique. Fig. 8 shows cyclic voltammetry (CV) plots of all three molecules. As seen in Fig. 8 a-c, the current increase in each cycle shows that all three molecules polymerized on the electrode surface and the coated polymer is conductive. When the first two cycles of the cyclic voltammetry graphs of the molecules have been examined in order to further elaborate the electropolymerization process, it has been observed that all molecules start oxidation at the different onset potentials in the first CV cycle. The onset potential for the M1 molecule has been observed at 0.62 V, whereas these values are 0.72 V and 0.60 V for M2 and M3 molecules, respectively. Change in onset potentials can be explained using the frontier molecular orbitals diagram in Fig. 4. The

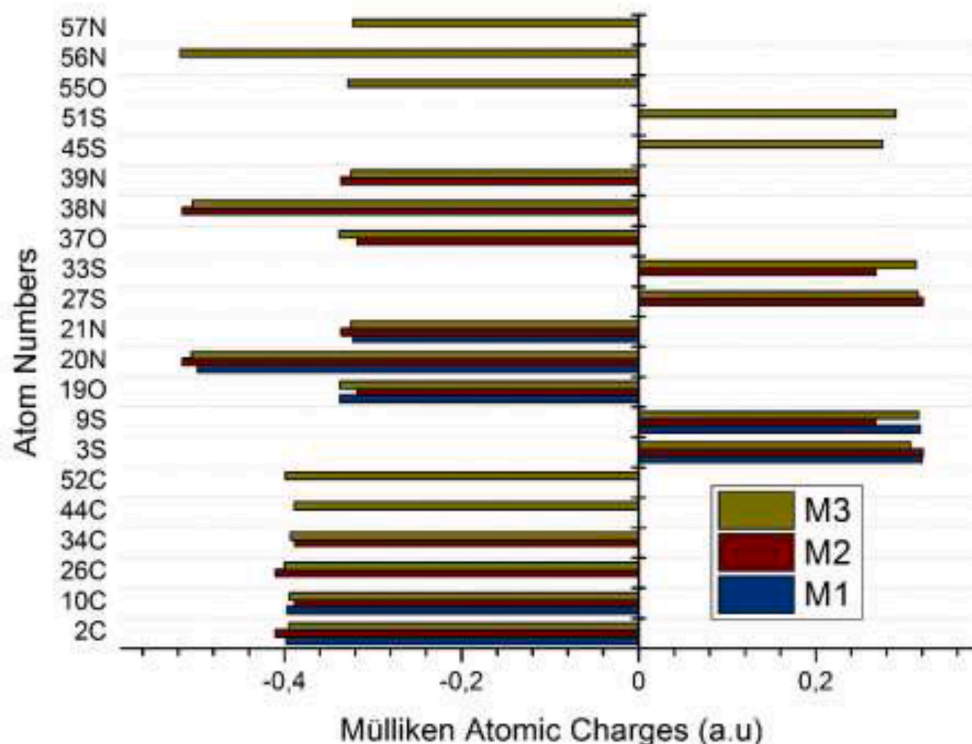


Fig. 6. Mulliken atomic charges of M1, M2 and M3 molecules, respectively.

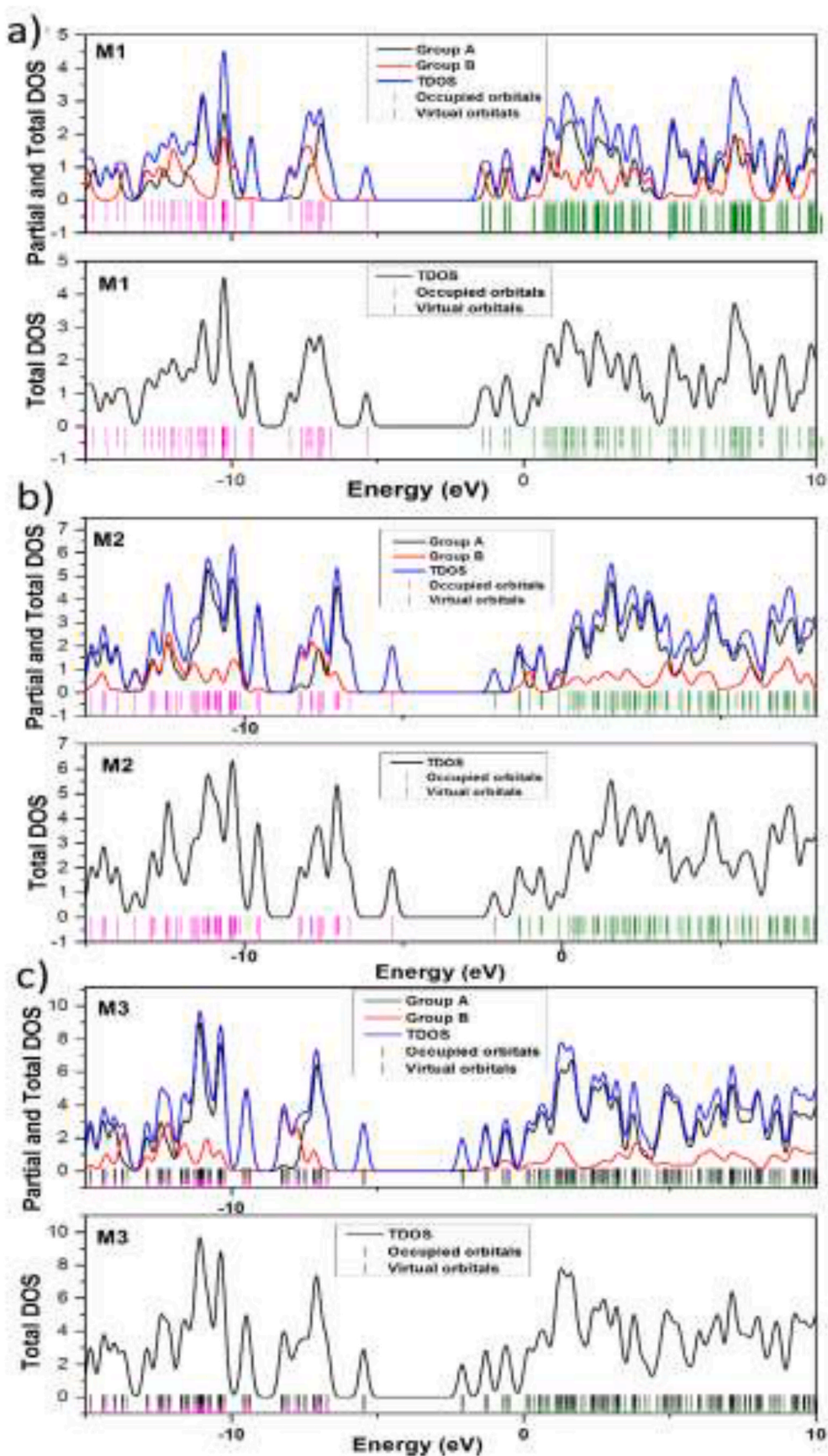


Fig. 7. Total density of states (TDOS), partial density of states analysis (PDOS) and band structures of a) M1, b) M2 and c) M3 molecules, respectively.

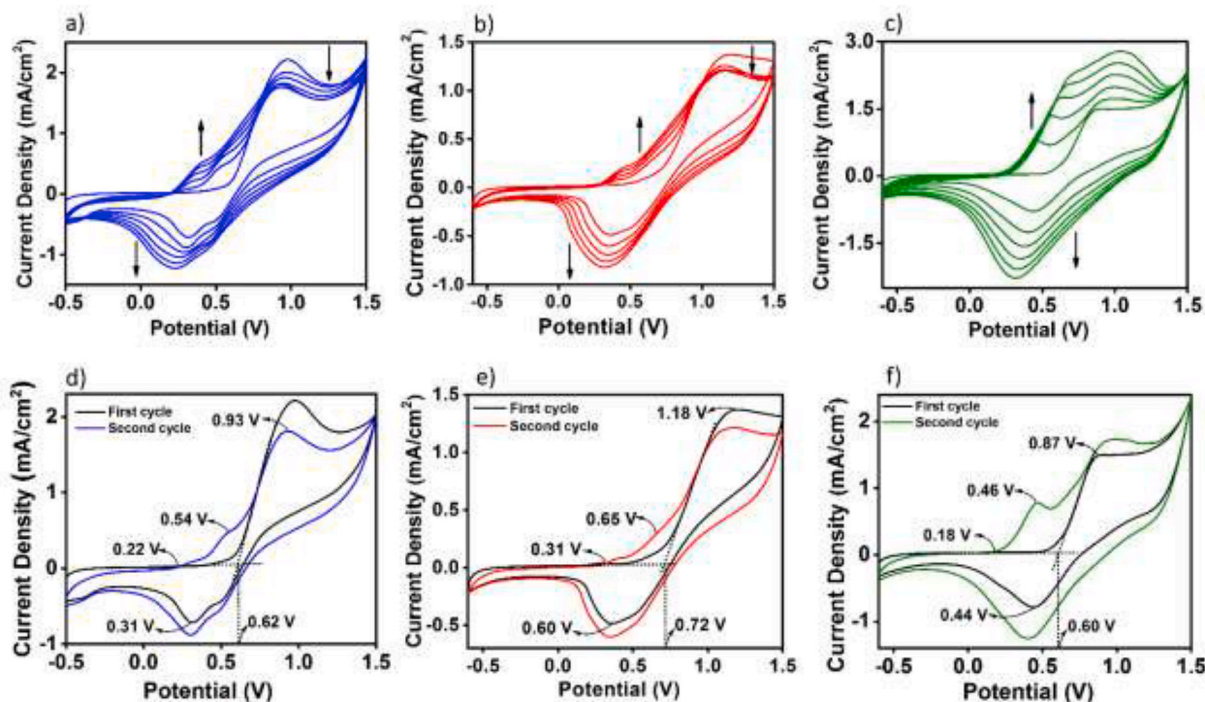


Fig. 8. Cyclic voltammetry of the a) M1, b) M2, c) M3 and first and second cycle of cyclic voltammograms of d) M1, e) M2 and f) M3 at 100 mV/s in 0.1 M ACN/LiClO<sub>4</sub>.

energy required in the oxidation and reduction of the examined molecules, is tightly related to the required energy to remove an electron from the HOMO level and released energy from addition of electron to the LUMO level, respectively. M3 has most easily oxidized and M2 has the biggest onset oxidation potential value as compatible with the result of DFT calculations. The difference between the onset potentials can also be explained by the three dimensional geometries of the molecules. Comparing the dihedral angles of optimized structures, it has been determined that the structure planarity is related with the onset potentials. Having the most planar 2,5-di(2-thienyl)-1H-pyrrole group, M3 has the lowest onset potential, while M2 with the most plane distortion has the highest onset potential. The reason for difference in onset potentials can be explained as the rotational disorder around single bonds that means the large dihedral angle between consecutive units limits the delocalization of  $\pi$ -electrons along the conjugated structure. Structure planarity affects not only onset potentials but also other redox properties. Redox properties such as monomer oxidation peak potentials, polymer oxidation peak potentials, and polymer oxidation onset potentials have exhibited regular change with respect to the planarity of the molecular structure.

Furthermore, Partial State Density (PDOS) calculations can provide excellent solutions for interpreting the redox behavior of molecules. As a result of PDOS calculations for the examined molecules, almost all the HOMO levels of each molecule are occupied by the 2,5-di(2-thienyl)-1H-pyrrole groups (Group A), and the LUMO is occupied by the rest of the structure (Group B). Thus, the 2,5-di(2-thienyl)-1H-pyrrole groups acts as an electron donor, while group B acts as an electron acceptor in all molecules. Since the electron donor property of the Group A in all molecules shows a tendency as  $M3 > M1 > M2$  from the PDOS calculations, redox properties such as onset potentials of the molecules have been affected from this tendency as shown in Table 3. Reversible charge storage capacity of conducting polymers make them good candidates for batteries, electrochromic devices, and supercapacitors applications. A simple explanation of the reason of charge density in CPs is that electrons are extracted from the HOMO of the valence band or transferred to the LUMO of the conduction band. This oxidation/reduction process

produces charge carriers in the form of polarons and bipolarons on the backbone of the CP. The charge densities of the examined molecules have been investigated by the cyclic voltammetry technique. For this purpose, conductive polymer films were synthesized on the ITO electrode with the oxidative polymerization technique detailed in the experimental part, and their cyclic voltammetry's have been taken in the 0.1 M LiClO<sub>4</sub>/ACN electrolyte solution in the range of  $-0.5/1.5$  V at 100 mV/s of scan rate (Fig. 9). Charge density values for M1, M2 and M3 have been calculated as 1.877, 1.741 and 3.264 mC/cm<sup>2</sup>, respectively. These values correspond to the area under the cyclic voltammetry curves and have been obtained by integrating of the curves in Fig. 9. Studies have shown that molecules with high dihedral angles have very low backbone planarity. This result probably caused the low charge density of polymer-based devices. In accordance with the literature, polymers of more planar molecules with low dihedral angles have a high charge density [72].

UV-vis spectroelectrochemical technique is the most suitable technique used to determine the spectrum of electronic transitions between the fundamental level and polaronic or bipolaronic levels of conductive polymers. Spectroelectrochemistry is used for the optical characterization of the conducting polymers under applied voltages. In this technique, a UV-vis spectrophotometer is combined with a potentiostat to examine changes optical properties of the polymer with applied potential. The recording of the spectrum during gradual reduction or oxidation provides useful information about optical band gap, polaronic and bipolaronic states. Spectroelectrochemical measurements have been made for polymer films coated on ITO quartz electrodes that immersed in a quartz cuvette containing electrolyte solution.

Fig. 10 a, b and c show spectroelectrochemical graphs for conductive polymers of M1, M2 and M3 molecules, respectively. Intense absorption corresponds to bipolaron bands have been observed in the spectrum of the oxidized states of the polymers at about 900 nm. Optical contrast values of the polymers at the bipolaron bands wavelength have been calculated as 32%, 94% and 65%, respectively. Optical contrast values of all polymers at both wavelength ( $\pi - \pi^*$  transition bands and bipolaron bands) have been observed to be compatible with each other as

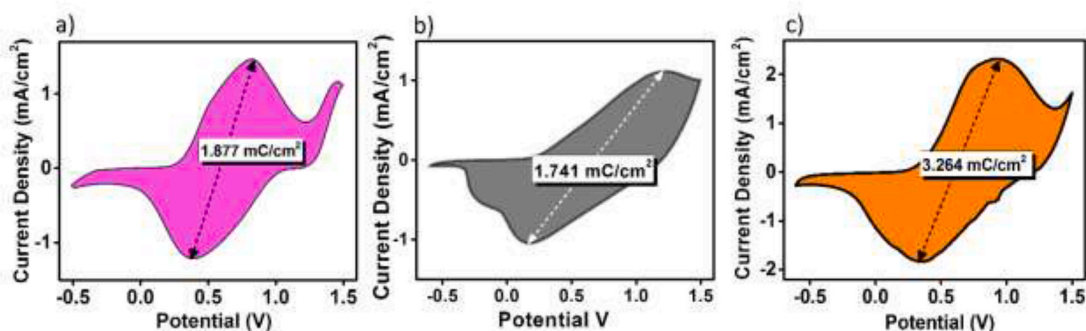


Fig. 9. Cyclic voltammetry studies of the conducting polymers obtained from a) M1, b) M2 and M3 to calculate charge density.

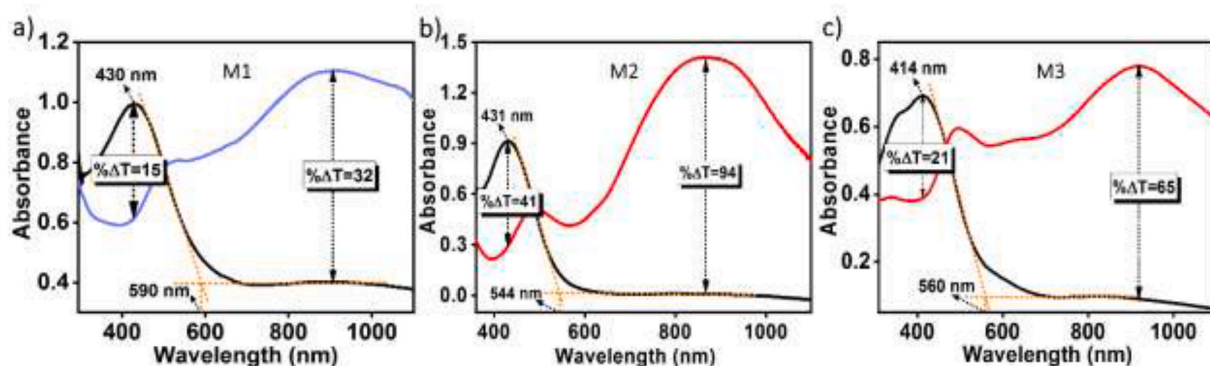


Fig. 10. Spectroelectrochemical investigations of the conducting polymers obtained by electrochemical polymerization of a) M1, b) M2 and c) M3.

optical contrast values at both wavelengths exhibited  $M1 < M3 < M2$  arrangement. From this result, it has been observed that the optical contrast values of the polymers are related to the magnitude of the band gap energy of the monomeric molecules. Conductive polymers obtained from 2,5-di(2-thienyl)-1H-pyrrole molecules with low band gap have been found to have high optical contrast values. Therefore, for this study, the optical contrast values of the conductive polymer obtained as a result of polymerization of molecules containing 2,5-di(2-thienyl)-1H-pyrrole can be increased by tuning the band gap energy of the monomeric molecules.

#### 4. Conclusion

In this study, the structural geometries and electronic properties of different monomeric structures with the same electroactive group have been investigated to provide a relationship between calculated electronic properties of the monomers with the observed optical and electrical properties of their conjugated polymers. For this purpose, three different amide substituted 2,5-di(2-thienyl)-1H-pyrrole compounds containing a different number of electroactive groups have been synthesized and molecular structure optimizations have been carried out with the DFT calculations. FT-IR and NMR spectra of optimized geometries have been compared with experimental data. The structural, spectroscopic and electronic properties of M1, M2 and M3 conductive polymers synthesized in this work are identified by performing the measurements of FT-IR,  $^1\text{H}$  NMR and  $^{13}\text{C}$  NMR spectra as well as quantum chemistry calculations based on DFT method. The geometries of the electroactive molecules titled as M1, M2, and M3 are optimized through DFT method at the level of B3LYP with basis set of 6-311G(d). The bond lengths, bond angles and dihedral angles are computed as structural properties by employing quantum computational methods. It has been observed that M3 and M1 molecules are more planar than M2 molecules by examining the geometrical structures of molecules

considering in this work. The fundamental vibrational modes of the multifunctional conjugated polymers are assigned. The vibrational frequencies computed from DFT method are compatible with the experimental results, since the regression coefficients goes to approximately unity. It is shown that the computational values of the harmonic frequencies deviate slightly from the experimental data. This disagreement may be due to ignoring the anharmonic effects and the general trend of the quantum chemical methods overestimating the force constants at the equilibrium geometry. The correlation between the calculation and experimental FT-IR data is provided by fitting our data to linear equations. The electronic properties of conjugated polymers synthesized in the present work are revealed by fulfilling frontier molecular analysis, electrostatic potential maps, Mulliken charge distribution, the total density of states, partial density of states analysis and band structures of the title molecules. It is observed that M1 molecule has less chemical reactivity than other molecules by analyzing the results of FMO. It is also shown that M3 molecule is the most electrophilic and reactive molecule than ones of other molecules. Moreover, it is seen that the electron density of M3 molecule is highest thanks to the electroactive regions by examining ESP maps and Mulliken charges analyses. The difference between the onset potentials have been explained by the three dimensional geometries of the molecules. Comparing the dihedral angles of optimized structures, it has been determined that the structure planarity is related with the onset potentials. Having the most planar 2,5-di(2-thienyl)-1H-pyrrole group, M3 has the lowest onset potential, while M2 with the most plane distortion has the highest onset potential. The reason for difference in onset potentials can be explained as the rotational disorder around single bonds that means the large dihedral angle between consecutive units limits the delocalization of  $\pi$ -electrons along the conjugated structure. Structure planarity affects not only onset potentials but also other redox properties such as monomer oxidation peak potentials, polymer oxidation peak potentials, and polymer oxidation onset potentials. Reversible charge storage capacity of conducting

polymers make them good candidates for batteries, electrochromic devices, and supercapacitors applications. Charge density studies have shown that molecules with high dihedral angles have very low backbone planarity and this probably caused the low charge density of polymer-based devices. In accordance with the literature, polymers of more planar molecules with low dihedral angles have a high charge density. Optical contrast values of all polymers at both wavelength ( $\pi$ - $\pi^*$  transition bands and bipolaron bands) have been observed to be compatible with each other as optical contrast values at both wavelengths exhibited M1<M3<M2 arrangement. From this result, it has been observed that the optical contrast values of the polymers are related to the magnitude of the band gap energy of the monomeric molecules. Conductive polymers obtained from 2,5-di(2-thienyl)-1H-pyrrole molecules with low band gap have been found to have high optical contrast values. Therefore, for this study, the optical contrast values of the conductive polymer obtained as a result of polymerization of molecules containing 2,5-di(2-thienyl)-1H-pyrrole can be increased by tuning the band gap energy of the monomeric molecules. As a result, optical and electrical properties of the conducting polymers can be controlled effectively with smart monomer design based on structure-property relationship approaches. In this point of view, quantum mechanical calculations have crucial role in designing of monomers and their conjugated polymers for desired optical and electrochemical properties.

### Declaration of competing interest

The authors declare that they have no known competing financial interests or personal relationships that could have appeared to influence the work reported in this paper.

### Acknowledgements

This study has been supported by Pamukkale University (Grant Nos: 2019FEBE050, 2019FEBE051).

### Appendix A. Supplementary data

Supplementary data to this article can be found online at <https://doi.org/10.1016/j.jpics.2020.109720>.

### References

- [1] L. Li, Y. Zhang, H. Lu, Y. Wang, J. Xu, J. Zhu, C. Zhang, T. Liu, Cryopolymerization enables anisotropic polyaniline hybrid hydrogels with superelasticity and highly deformation-tolerant electrochemical energy storage, *Nat. Commun.* 11 (2020) 62, <https://doi.org/10.1038/s41467-019-13959-9>.
- [2] P. Camurlu, S. Tarku, E. Şahmetlioğlu, İ.M. Akhmedov, C. Tanyeli, L. Toppare, Multichromic conducting copolymer of 1-benzyl-2,5-di(thiophen-2-yl)-1H-pyrrole with EDOT, *Sol. Energy Mater. Sol. Cells* 92 (2008) 154–159, <https://doi.org/10.1016/j.solmat.2006.12.020>.
- [3] P. Camurlu, Polypyrrole derivatives for electrochromic applications, *RSC Adv.* 4 (2014) 55832–55845, <https://doi.org/10.1039/C4RA11827H>.
- [4] T. Soganci, M. Ak, An eco-friendly method to enhance optical and electrical properties of conducting polymers by means of carboxymethyl cellulose, *Cellulose* 26 (2019) 2541–2555, <https://doi.org/10.1007/s10570-019-02248-9>.
- [5] B.C. Ozkan, T. Soganci, H. Turhan, M. Ak, Investigation of rGO and chitosan effects on optical and electrical properties of the conductive polymers for advanced applications, *Electrochim. Acta* 295 (2019) 1044–1051, <https://doi.org/10.1016/j.electacta.2018.11.032>.
- [6] M. Guzel, E. Karataş, M. Ak, A new way to obtain black electrochromism: appropriately covering whole visible regions by absorption spectra of copolymers composed of EDOT and carbazole derivatives, *Smart Mater. Struct.* 28 (2019), 025013, <https://doi.org/10.1088/1361-665X/aaf1e3>.
- [7] R. Ayranci, F.O. Kirbay, D.O. Demirkol, M. Ak, S. Timur, Copolymer based multifunctional conducting polymer film for fluorescence sensing of glucose, *Methods Appl. Fluoresc.* 6 (2018), 035012, <https://doi.org/10.1088/2050-6120/aac519>.
- [8] M. Ak, P. Camurlu, F. Yılmaz, L. Cianga, Y. Yağcı, L. Toppare, Electrochromic properties and electrochromic device application of copolymer ofN-(4-(3-thienyl methylene)-oxycarbonylphenyl)maleimide with thiophene, *J. Appl. Polym. Sci.* 102 (2006) 4500–4505, <https://doi.org/10.1002/app.24834>.
- [9] M. Ak, T. Soganci, Chapter 10. Electrochemical properties and electrochromic device applications of polycarbazole derivatives, in: K.W.S. Jian Wei Xu, Ming

- Hui Chua (Eds.), *Electrochromic Smart Mater. Fabr. Appl.*, First, The Royal Society of Chemistry, London, 2019, pp. 293–322, <https://doi.org/10.1039/9781788016667-00293>, 2019.
- [10] S. Soyleyici, M. Karakus, M. Ak, Transparent-blue colored dual type electrochromic device: switchable glass application of conducting organic-inorganic hybrid carbazole polymer, *J. Electrochem. Soc.* 163 (2016) H679–H683, <https://doi.org/10.1149/2.0711608jes>.
- [11] T. Soganci, S. Soyleyici, H.C. Soyleyici, M. Ak, High contrast electrochromic polymer and copolymer materials based on amide-substituted poly(dithienyl pyrrole), *J. Electrochem. Soc.* 164 (2017) H11–H20, <https://doi.org/10.1149/2.0111702jes>.
- [12] T. Soganci, O. Gumusay, H.C. Soyleyici, M. Ak, Synthesis of highly branched conducting polymer architecture for electrochromic applications, *Polymer* 134 (2018) 187–195, <https://doi.org/10.1016/j.polymer.2017.11.067>.
- [13] M. Guzel, T. Soganci, R. Ayranci, M. Ak, Smart windows application of carbazole and triazine based star shaped architecture, *Phys. Chem. Chem. Phys.* 18 (2016) 21659–21667, <https://doi.org/10.1039/C6CP2611G>.
- [14] C.-H. Huang, Z.-Y. Chen, C.-L. Chiu, T.-T. Huang, H.-F. Meng, P. Yu, Surface micro-/nanotextured hybrid PEDOT:PSS-silicon photovoltaic cells employing Kirigami Graphene, *ACS Appl. Mater. Interfaces* 11 (2019) 29901–29909, <https://doi.org/10.1021/acsami.9b08366>.
- [15] S. Park, M.J. Cha, J.H. Seo, J. Heo, D. Chan Lim, S. Cho, Treating the poly(3,4-ethylenedioxythiophene):poly(styrenesulfonate) surface with hydroquinone enhances the performance of polymer solar cells, *ACS Appl. Mater. Interfaces* 10 (2018) 41578–41585, <https://doi.org/10.1021/acsami.8b15551>.
- [16] S. Kommeren, M.J.J. Coenen, T.M. Eggenhuisen, T.W.L. Slaats, H. Gorter, P. Groen, Combining solvents and surfactants for inkjet printing PEDOT:PSS on P3HT/PCBM in organic solar cells, *Org. Electron.* 61 (2018) 282–288, <https://doi.org/10.1016/j.orgel.2018.06.004>.
- [17] D. Wagner, S.T. Hoffmann, U. Heinemeyer, I. Münster, A. Köhler, P. Strohriegel, Triazine based bipolar host materials for blue phosphorescent OLEDs, *Chem. Mater.* 25 (2013) 3758–3765, <https://doi.org/10.1021/cm4023216>.
- [18] Y. Mizuno, I. Takasu, S. Uchikoga, S. Enomoto, T. Sawabe, A. Amano, A. Wada, T. Sugizaki, J. Yoshida, T. Ono, C. Adachi, Fluorinated carbazole derivatives as wide-energy-gap host material for blue phosphorescent organic light-emitting diodes, *J. Phys. Chem. C* 116 (2012) 20681–20687, <https://doi.org/10.1021/jp303085h>.
- [19] F. Ghorbani Zamani, H. Moulahoum, M. Ak, D. Odaci Demirkol, S. Timur, Current trends in the development of conducting polymers-based biosensors, *TrAC Trends Anal. Chem. (Reference Ed.)* 118 (2019) 264–276, <https://doi.org/10.1016/j.trac.2019.05.031>.
- [20] T. Soganci, H.C. Soyleyici, M. Ak, Fabrication of multifunctional 2,5-di(2-thienyl) pyrrole based conducting copolymer for further sensor and optoelectronic applications, *J. Electrochem. Soc.* 165 (2018) H941–H953, <https://doi.org/10.1149/2.0811814jes>.
- [21] R. Ayranci, M. Ak, An electrochemical sensor platform for sensitive detection of iron (III) ions based on pyrene-substituted poly(2,5-dithienylpyrrole), *J. Electrochem. Soc.* 166 (2019) B291–B296, <https://doi.org/10.1149/2.0101906jes>.
- [22] G. Oyman, C. Geyik, R. Ayranci, M. Ak, D. Odaci Demirkol, S. Timur, H. Coskunol, Peptide-modified conducting polymer as a biofunctional surface: monitoring of cell adhesion and proliferation, *RSC Adv.* 4 (2014) 53411–53418, <https://doi.org/10.1039/C4RA08481K>.
- [23] T.Y. Tekbaşoğlu, T. Soganci, M. Ak, A. Koca, M.K. Şener, Enhancing biosensor properties of conducting polymers via copolymerization: synthesis of EDOT-substituted bis(2-pyridylimino)isoindolato-palladium complex and electrochemical sensing of glucose by its copolymerized film, *Biosens. Bioelectron.* 87 (2017) 81–88, <https://doi.org/10.1016/j.bios.2016.08.020>.
- [24] R. Olgae, T. Soganci, Y. Baygu, Y. Gök, M. Ak, Zinc(II) phthalocyanine fused in peripheral positions octa-substituted with alkyl linked carbazole: synthesis, electropolymerization and its electro-optic and biosensor applications, *Biosens. Bioelectron.* 98 (2017) 202–209, <https://doi.org/10.1016/j.bios.2017.06.028>.
- [25] T. Soganci, Y. Baygu, N. Kabay, Y. Gök, M. Ak, Comparative investigation of peripheral and nonperipheral zinc phthalocyanine-based polycarbazoles in terms of optical, electrical, and sensing properties, *ACS Appl. Mater. Interfaces* 10 (2018) 21654–21665, <https://doi.org/10.1021/acsami.8b06206>.
- [26] R. Ayranci, D.O. Demirkol, S. Timur, M. Ak, Rhodamine-based conjugated polymers: potentiometric, colorimetric and voltammetric sensing of mercury ions in aqueous medium, *Analyst* 142 (2017) 3407–3415, <https://doi.org/10.1039/C7AN00606C>.
- [27] R. Ayranci, Y. Torlak, T. Soganci, M. Ak, Trilacunary Keggin type polyoxometalate-conducting polymer composites for amperometric glucose detection, *J. Electrochem. Soc.* 165 (2018) B638–B643, <https://doi.org/10.1149/2.1061813jes>.
- [28] R. Yuksel, S. Coskun, G. Gunbas, A. Cirpan, L. Toppare, H.E. Unalan, Silver nanowire/conducting polymer nanocomposite electrochromic supercapacitor electrodes, *J. Electrochem. Soc.* 164 (2017) A721–A727, <https://doi.org/10.1149/2.0791704jes>.
- [29] G.M. Suppes, B.A. Deore, M.S. Freund, Porous conducting polymer/heteropolyoxometalate hybrid material for electrochemical supercapacitor applications, *Langmuir* 24 (2008) 1064–1069, <https://doi.org/10.1021/la702837j>.
- [30] S.Y. Son, Y. Kim, J. Lee, G.-Y. Lee, W.-T. Park, Y.-Y. Noh, C.E. Park, T. Park, High-field-effect mobility of low-crystallinity conjugated polymers with localized aggregates, *J. Am. Chem. Soc.* 138 (2016) 8096–8103, <https://doi.org/10.1021/jacs.6b01046>.

- [31] M. Moral, A. Garzón, J. Canales-Vázquez, J.C. Sancho-García, Optoelectronic and semiconducting properties of conjugated polymers composed of thiazolo[5,4-d] thiazole and arene imides linked by ethynylene bridges, *J. Phys. Chem. C* 120 (2016) 24583–24596, <https://doi.org/10.1021/acs.jpcc.6b07240>.
- [32] S.-K. Pang, Comprehensive study of polymerization of pyrrole: a theoretical approach, *J. Electroanal. Chem.* 859 (2020) 113886, <https://doi.org/10.1016/j.jelechem.2020.113886>.
- [33] H. Xiao, X. Zhang, J.-Y. Wang, L.-Y. Zhang, Q.-C. Zhang, Z.-N. Chen, Enhancing phosphorescence through rigidifying the conformation to achieve high-efficiency OLEDs by modified PEDOT, *ACS Appl. Mater. Interfaces* 11 (2019) 45853–45861, <https://doi.org/10.1021/acsami.9b15807>.
- [34] P.E. Rudnicki, Q. MacPherson, L. Balhorn, B. Feng, J. Qin, A. Salles, A. J. Spakowitz, Impact of liquid-crystalline chain alignment on charge transport in conducting polymers, *Macromolecules* 52 (2019) 8932–8939, <https://doi.org/10.1021/acs.macromol.9b01729>.
- [35] S.Ö. Kart, A. Ebru Tanboğa, H.C. Soyleyici, M. Ak, H.H. Kart, Theoretical study of the structure–properties relationship in new class of 2,5-di(2-thienyl)pyrrole compounds, *Spectrochim. Acta Part A Mol. Biomol. Spectrosc.* 137 (2015) 1174–1183, <https://doi.org/10.1016/j.saa.2014.08.143>.
- [36] A.Ö. Kiraz, İ. Kara, M. Ak, H. Çetişli, N. Kolsuz, Theoretical investigation of triazine based a star shape pyrrole monomer, *J. Macromol. Sci. Part A* 54 (2017) 16–23, <https://doi.org/10.1080/10601325.2017.1250310>.
- [37] D.B. Boyd, Successes of computer-assisted molecular design, in: *rev. Comput. Chem.* (2007) 355–371, <https://doi.org/10.1002/9780470125786.ch10>.
- [38] H. Pir, N. Günay, D. Avci, Y. Atalay, Molecular structure, vibrational spectra, NLO and NBO analysis of bis(8-oxy-1-methylquinolinium) hydroiodide, *Spectrochim. Acta Part A Mol. Biomol. Spectrosc.* 96 (2012) 916–924, <https://doi.org/10.1016/j.saa.2012.07.044>.
- [39] M. Kamran, H. Ullah, A.-H.A. Shah, S. Bilal, A.A. Tahir, K. Ayub, Combined experimental and theoretical study of poly(aniline-co-pyrrole) oligomer, *Polymer* 72 (2015) 30–39, <https://doi.org/10.1016/j.polymer.2015.07.003>.
- [40] S. Yang, P. Olishovski, M. Kertesz, Bandgap calculations for conjugated polymers, *Synth. Met.* 141 (2004) 171–177, <https://doi.org/10.1016/j.synthmet.2003.08.019>.
- [41] H. Nikoofard, H.N. Jobi, Theoretical study of 1-amino-9,10-anthraquinone oligomers: structural, electronic, and UV–visible spectral properties, *J. Mol. Struct.* 1191 (2019) 138–144, <https://doi.org/10.1016/j.molstruc.2019.04.089>.
- [42] M. Ak, M.S. Ak, L. Toppare, Electrochemical properties of a new star-shaped pyrrole monomer and its electrochromic applications, *Macromol. Chem. Phys.* 207 (2006) 1351–1358, <https://doi.org/10.1002/macp.200600178>.
- [43] T. Soganci, S. Soyleyici, H.C. Soyleyici, M. Ak, Optoelectrochromic characterization and smart windows application of bi-functional amid substituted thienyl pyrrole derivative, *Polymer* 118 (2017) 40–48, <https://doi.org/10.1016/j.polymer.2017.04.060>.
- [44] T. Soganci, H.C. Soyleyici, E. Gizirolu, M. Ak, Processable amide substituted 2,5-Bis(2-thienyl)pyrrole based conducting polymer and its fluorescent and electrochemical properties, *J. Electrochem. Soc.* 163 (2016) H1096–H1103, <https://doi.org/10.1149/2.0071614jes>.
- [45] M.J. Frisch, G.W. Trucks, H.B. Schlegel, G.E. Scuseria, M.A. Robb, J.R. Cheeseman, G. Scalmani, V. Barone, G.A. Petersson, H. Nakatsuji, X. Li, M. Caricato, A. Marenich, J. Bloino, B.G. Janesko, R. Gomperts, B. Mennucci, H.P. Hratchian, J. V. Ortiz, A.F. Izmaylov, J.L. Sonnenberg, D. Williams-Young, F. Ding, F. Lipparini, F. Egidi, J. Goings, B. Peng, A. Petrone, T. Henderson, D. Ranasinghe, V. G. Zakrzewski, J. Gao, N. Rega, G. Zheng, W. Liang, M. Hada, M. Ehara, K. Toyota, R. Fukuda, J. Hasegawa, M. Ishida, T. Nakajima, Y. Honda, O. Kitao, H. Nakai, T. Vreven, K. Throssell, J.A. Montgomery Jr., J.E. Peralta, F. Ogliaro, M. Bearpark, J.J. Heyd, E. Brothers, K.N. Kudin, V.N. Staroverov, T. Keith, R. Kobayashi, J. Normand, K. Raghavachari, A. Rendell, J.C. Burant, S.S. Iyengar, J. Tomasi, M. Cossi, J.M. Millam, M. Klene, C. Adamo, R. Cammi, J.W. Ochterski, R.L. Martin, K. Morokuma, O. Farkas, J.B. Foresman, D.J. Fox, *Gaussian 09, Rev. D.01*, Gaussian Inc., Wallingford, CT, 2016.
- [46] H.C. Soyleyici, M. Ak, Y. Şahin, D.O. Demikol, S. Timur, New class of 2,5-di(2-thienyl)pyrrole compounds and novel optical properties of its conducting polymer, *Mater. Chem. Phys.* 142 (2013) 303–310, <https://doi.org/10.1016/j.matchemphys.2013.07.019>.
- [47] İ. Yağmur, M. Ak, A. Bayrakçeken, Fabricating multicolored electrochromic devices using conducting copolymers, *Smart Mater. Struct.* 22 (2013) 115022, <https://doi.org/10.1088/0964-1726/22/11/115022>.
- [48] R. Dennington, T. Keith, J. Millam, GaussView, Version 5, Semichem Inc., Shawnee Mission, KS, 2009.
- [49] M.H. Jamróz, Vibrational energy distribution analysis (VEDA): scopes and limitations, *spectrochim. Acta Part A Mol. Biomol. Spectrosc.* 114 (2013) 220–230, <https://doi.org/10.1016/j.saa.2013.05.096>.
- [50] A.D. Becke, Density-functional exchange-energy approximation with correct asymptotic behavior, *Phys. Rev. B* 38 (1988) 3098–3100, <https://doi.org/10.1103/PhysRevB.38.3098>.
- [51] A.D. Becke, Density-functional thermochemistry. III. The role of exact exchange, *J. Chem. Phys.* 98 (1993) 5648–5652, <https://doi.org/10.1063/1.464913>.
- [52] J. Roncali, Molecular engineering of the band gap of  $\pi$ -conjugated systems: facing technological applications, *Macromol. Rapid Commun.* 28 (2007) 1761–1775, <https://doi.org/10.1002/marc.200700345>.
- [53] R.D. Johnson III, NIST computational chemistry comparison and benchmark database NIST standard reference database number 101, *Comput. Chem. Comp. Benchmark Database NIST Stand. Ref. Database Number 101* (2018), <https://doi.org/10.18434/T47C7Z>.
- [54] S. Sieber, P.v.R. Schleyer, J. Gauss, The accurate C2v phenonium and benzenonium ion structures confirmed by correlated GIAO-MP2 NMR chemical shift calculations, *J. Am. Chem. Soc.* 115 (1993) 6987–6988, <https://doi.org/10.1021/ja00068a072>.
- [55] K.B. Wiberg, Comparison of density functional theory models' ability to reproduce experimental 13C-NMR shielding values, *J. Comput. Chem.* 20 (1999) 1299–1303, [https://doi.org/10.1002/\(SICI\)1096-987X\(199909\)20:12<1299::AID-JCC10>3.0.CO;2-F](https://doi.org/10.1002/(SICI)1096-987X(199909)20:12<1299::AID-JCC10>3.0.CO;2-F).
- [56] K. Fukui, Role of frontier orbitals in chemical reactions, *Science* 218 (1982) 747–754, <https://doi.org/10.1126/science.218.4574.747>, 80.
- [57] T. Koopmans, Über die Zuordnung von Wellenfunktionen und Eigenwerten zu den Einzelnen Elektronen Eines Atoms, *Physica* 1 (1934) 104–113, [https://doi.org/10.1016/S0031-8914\(34\)90011-2](https://doi.org/10.1016/S0031-8914(34)90011-2).
- [58] R.G. Pearson, Absolute electronegativity and hardness correlated with molecular orbital theory, *Proc. Natl. Acad. Sci. Unit. States Am.* 83 (1986) 8440–8441, <https://doi.org/10.1073/pnas.83.22.8440>.
- [59] I. Fleming, *Molecular Orbitals and Organic Chemical Reactions*, John Wiley & Sons, Ltd, Chichester, UK, UK, 2009, <https://doi.org/10.1002/9780470684306>.
- [60] P. Politzer, J.S. Murray, The fundamental nature and role of the electrostatic potential in atoms and molecules, *Theor. Chem. Accounts Theor. Comput. Model.* 108 (2002) 134–142, <https://doi.org/10.1007/s00214-002-0363-9>.
- [61] M. Evecen, H. Tanak, F. Timmaz, N. Dege, İ. Ozer İlhan, Experimental (XRD, IR and NMR) and theoretical investigations on 1-(2-nitrobenzoyl)3,5-bis(4-methoxyphenyl)-4,5-dihydro-1H-pyrazole, *J. Mol. Struct.* 1126 (2016) 117–126, <https://doi.org/10.1016/j.molstruc.2016.01.069>.
- [62] A.E. Reed, R.B. Weinstock, F. Weinhold, Natural population analysis, *J. Chem. Phys.* 83 (1985) 735–746, <https://doi.org/10.1063/1.449486>.
- [63] A.E. Reed, F. Weinhold, Some remarks on the C–H bond dipole moment, *J. Chem. Phys.* 84 (1986) 2428–2430, <https://doi.org/10.1063/1.450359>.
- [64] J. Prashanth, G. Ramesh, J. Laxman Naik, J. Kishan Ojha, B. Venkatram Reddy, Molecular geometry, NBO analysis, Hyperpolarizability and HOMO-LUMO energies of 2-azido-1-phenylethanol using Quantum chemical calculations, *Mater. Today Proc.* 3 (2016) 3761–3769, <https://doi.org/10.1016/j.matpr.2016.11.025>.
- [65] M. Evecen, H. Tanak, Molecular and electronic analysis of (7-chloro-2-oxo-2H-chromen-4-yl)-methyl diethylcarbamodithioate by DFT and HF calculations, *Acta Phys. Pol.* A 136 (2019) 3–17, <https://doi.org/10.12693/APhysPolA.136.3>.
- [66] S.C. Jeyaseelan, R. Premkumar, K. Kaviyarasu, A.M. Franklin Benial, Spectroscopic, quantum chemical, molecular docking and in vitro anticancer activity studies on 5-Methoxyindole-3-carboxaldehyde, *J. Mol. Struct.* 1197 (2019) 134–146, <https://doi.org/10.1016/j.molstruc.2019.07.042>.
- [67] M. Kavimani, V. Balachandran, B. Narayana, K. Vanasundari, B. Revathi, Topological analysis (BCP) of vibrational spectroscopic studies, docking, RDG, DSSC, Fukui functions and chemical reactivity of 2-methylphenylacetic acid, *Spectrochim. Acta Part A Mol. Biomol. Spectrosc.* 190 (2018) 47–60, <https://doi.org/10.1016/j.saa.2017.09.005>.